

# Half-lives for proton emission, alpha decay, cluster radioactivity, and cold fission processes calculated in a unified theoretical framework

*S. B. Duarte, O. A. P. Tavares, F. Guzmán\*, A. Dimarco*

Centro Brasileiro de Pesquisas Físicas—CBPF/MCT  
Rua Dr. Xavier Sigaud 150, 22290-180 Rio de Janeiro—RJ, Brazil

*F. García† and O. Rodríguez\**

Instituto de Física, Universidade de São Paulo,  
Caixa Postal 66318, 05315-970 São Paulo—SP, Brazil

*M. Gonçalves*

Instituto de Radioproteção e Dosimetria—IRD/CNEN  
Av. Salvador Allende s/n, 22780-160 Rio de Janeiro—RJ, Brazil

**Abstract.** Half-life values of spontaneous nuclear decay processes are presented in the framework of the Effective Liquid Drop Model (ELDM) using the combination of varying mass asymmetry shape description for the mass transfer with Werner-Wheeler's inertia coefficient  $V_{MAS}/WW$ . The calculated half-lives of ground-state to ground-state transitions for the proton emission, alpha decay, cluster radioactivity, and cold fission processes are compared with experimental data. Results have shown that the ELDM is a very efficient model to describe these different decay processes in a same, unified theoretical framework. A Table listing the predicted half-life values,  $\tau_c$ , is presented for all possible cases of spontaneous nuclear break-up such that  $-7.30 \lesssim \log_{10} \tau_c [s] \lesssim 27.50$  and  $\log_{10}(\tau/\tau_c) > -17.0$ , where  $\tau$  is the total half-life of the parent nucleus.

**Key-words:** Proton emission; Alpha decay; Cluster radioactivity; Cold fission; Effective liquid drop model; Calculated half-life.

---

\*Permanent address: Instituto Superior de Ciencias y Tecnologia Nucleares, Av. Salvador Allende y Luaces, Ap. Postal 6163, La Habana, Cuba.

†Permanent address: Departamento de Ciências Exatas e Tecnológicas, Universidade Estadual de Santa Cruz, 45650-000 Ilhéus-Ba, Brazil.

## CONTENTS

Introduction	1
Shape parametrization and potential barrier	3
Gamow's factor and decay half-life	5
Nuclear radii and inertia coefficients	6
Comparison with experiment	8
Explanation of table	32
Table : Calculated $Q$ -values and half-lives for the most probable ground-state to ground-state hadronic decays of nuclei throughout the Periodic Table	33

## INTRODUCTION

Pioneering studies on spontaneous radioactive processes have considered the alpha decay and fission as completely different phenomena from each other concerning the internal nuclear structure. However, during the 80's this concept was changed after the first reporting on the possible occurrence of a very asymmetric mass splitting of heavy nuclei [1–3], and the subsequent discovery of a new spontaneous decay process, namely, the cluster radioactivity [4,5]. Theoretical predictions of the half-life for this new nuclear radioactive decay mode have been made, on one hand, in the framework of the fragmentation theory [6–8] based on the two-center shell model [9,10]. The idea has been constrained to the cold rearrangements of a large number of nucleons in the ground state of the parent nucleus. On the other hand, the cluster radioactivity process has been interpreted differently in terms of a clustering pre-formation followed by the fragment emission. In these treatments the emission of light clusters such as  $^{14}\text{C}$  has been interpreted in terms of ‘cluster-like decay’ [11–13], while for heavier fragment emission modes ( $^{24}\text{Ne}$ ,  $^{30}\text{Mg}$ ,  $^{34}\text{Si}$ , and  $^{48}\text{Ca}$ ) the interpretation has followed the ‘fission-like approach’. A systematic investigation of the new decay modes based on the analytical superasymmetric fission model (ASAFM) by Poenaru *et al* [14] revealed a number of nuclides with  $Z \geq 40$  which are found to be metastable with respect to heavy-ion emission modes. The ASAFM, which takes into account even-odd effects, was subsequently updated, also to include superheavy nuclei and nuclei far off the beta-stability valley [15].

In the early 90's a new fission process was observed for the first time as being due to the emission of two fragments of comparable masses in their ‘cold’ ground state, therefore with no neutron emission—the so-called cold fission process [16]. The occurrence of cold fission is also related to shell effects on the barrier, and the total kinetic energy of the final

fragments practically exhausts the  $Q$ -value for the process. Several theoretical descriptions have appeared to treat these three processes (alpha decay, cluster radioactivity, and cold fission) within a same theoretical framework, as a manifestation of structure effects such as the shell corrections, and the pairing and symmetry energy effects [17–26]. During this decade or so, nuclear cold fission and cluster radioactivity processes have been explored intensively from both the experimental and theoretical point of views [17–19,27–30]. The newest, available cold fission data are from the decay of  $^{230}\text{Th}$  [31],  $^{236,238,240,242,244}\text{Pu}$  [31–33],  $^{248}\text{Cm}$  [28],  $^{252}\text{Cf}$  [34–36], and  $^{233,234}\text{U}$  [31,37] isotopes.

Nowadays special attention has been dedicated to new nuclear properties that can be deduced from the processes of proton radioactivity and alpha decay observed in the region of proton-rich nuclei. Indeed, the competition between the spontaneous proton emission and alpha decay [38] is a promising tool for the analysis of possible peculiarities in the structure of these proton-rich nuclei [38–51], and also of great interest to the rapid proton-capture astrophysical nucleosynthesis, namely the rp-process. At present, there are few calculations, based mainly on Hartree-Fock [52], Hartree-Fock-Bogoliubov [53], and the effective liquid drop theory [54] to describe the nuclear structure and/or to calculate the half-life for the proton radioactivity process.

The effective liquid drop model (ELDM), formerly developed to describe the alpha decay and cluster radioactivity processes in a unified framework [13,26], has been extended to include the cold fission process, and also to discuss the effect of different inertia coefficients on the calculated half-lives and product mass yield distributions. It has been already shown that the half-life results calculated by using such a model depend strongly on the prescription employed to describe the changing of the mass asymmetry parameter during the scission process. However, we have demonstrated that by re-defining appropriately the values for the model parameters we can reach good agreement with the existing data [21,23,24]. This agreement has been observed for the alpha decay [22] and cluster radioactivity [23] processes, both for the earlier data [13,26] and the most recent data, where a new region of daughter nuclei around the double-magic  $^{100}\text{Sn}_{50}$  and  $^{132}\text{Sn}_{82}$  nuclei is expected to occur [21,26,55,56]. As a matter of fact, we have used our model to predict some new valleys of instability which would provide double-magic daughter nuclei in the region of  $^{100}\text{Sn}_{50}$  proton rich nucleus [21]. Results have pointed out that, besides the probable  $^{12}\text{C}$  cluster radioactivity, other emitted nuclei such as  $^{14}\text{N}$  and  $^{16}\text{O}$  can also lead to double-magic shell daughter nuclei [21].

In the limit of smallest fragment emission our model can deal also with the proton emission phenomenon, giving predicted half-life-values for several proton emitter nuclei in excellent agreement with the recent data [54]. Therefore, we can state that the present

ELDM, although being semi-classical in character, has shown to be a valuable tool in predicting of half-lives for the different nuclear decay processes in a unified theoretical framework.

The aim of this work is to update the half-life estimations for the proton emission, alpha decay, cluster radioactivity, and spontaneous cold fission processes within the ELDM by using the most recent atomic mass data tables by Audi *et al.* [57] and Möller *et al.* [58] as input data. In the next sections we detail the most relevant aspect of the model we are using, and the results and comments are presented in the last section. All decay cases within the limits of measurable half-life are displayed in a Table.

### SHAPE PARAMETRIZATION AND POTENTIAL BARRIER

According to the ELDM, a spherical, molecular shape has been established in order to obtain analytical expressions for the Coulomb and surface potential energies to calculate the total potential barrier. Gamow's penetrability factor [59] has been calculated by considering two different inertia coefficients: Werner-Wheeler's [60] and the effective inertia coefficients [26].

During the molecular phase of the process the geometrical configuration of the deformed system is approximated by two intersecting spheres of different radii. For the complete specification of this configuration we need four independent coordinates, disregarding the location of the center of mass of the system. Figure 1 shows a sketch of a typical configuration, where the choice for the coordinates are specified: the radii of each spherical segment,  $R_1$  and  $R_2$ , the height of the largest spherical segment,  $\xi$ , and the distance between their geometric centers,  $\zeta$ . At the end of the molecular phase the system reaches a limiting configuration of two spherical, tangent fragments with radii  $\bar{R}_1$  and  $\bar{R}_2$ , respectively, for the emitted fragment and daughter nucleus.

Three constraints have been introduced to reduce from the spherical four-dimensional problem to the equivalent one-dimensional one. To preserve the adopted shape parametrization for the deformed nuclear system during the molecular phase, i. e., to keep the spherical segments in contact, it is necessary to establish a geometric constraint,

$$R_1^2 - (\zeta - \xi)^2 = R_2^2 - \xi^2. \quad (1)$$

Since we are considering the incompressibility of the nuclear matter, the constraint for conservation of total volume of the system is expressed in our coordinates by

$$2(R_1^3 + R_2^3) + 3 [R_1^2(\zeta - \xi) + R_2^2\xi] - [(\zeta - \xi)^3 + \xi^3] = 4R_p^3, \quad (2)$$

where  $R_p$  is the radius of the parent nucleus.

The third constraint is associated with the flux of mass through the window connecting the two spheroids [see Fig. 1]. During the evolution of the molecular phase of fragments we are able to take a constant radius for the spherical segment corresponding to the nascent cluster, i.e., we have fixed  $R_1 = \bar{R}_1$ , or a constant volume for both fragments as established by Eq. (2). We will return to this point later, when discussing the inertia associated with the degree of freedom of the relative motion subjected to the constrained relationships mentioned above.

The model considers explicitly the Coulomb and surface energy contributions to the potential barrier. In our calculation we have used Gaudin's expression [61] for the electrostatic energy of two overlapping spherical segments with a uniform charge distribution,

$$V_c = \frac{8}{9}\pi a^5 \varepsilon(x_1, x_2) \rho_c, \quad (3)$$

where  $\rho_c$  is the initial charge density,  $\varepsilon$  is a function of the angular variables  $x_1$  and  $x_2$ , and  $a$  is the radius of the sharp neck. The variables  $x_1 = \pi - \theta_1$  and  $x_2 = \theta_2 - \pi$  are defined in terms of the angles  $\theta_1$  and  $\theta_2$ , shown in Fig. 1.

The expression for the  $\varepsilon$  factor in terms of the auxiliary functions  $f$ ,  $f'$  and  $g$  reads

$$\begin{aligned} \varepsilon(x_1, x_2) = & \left[ \frac{1}{\sin^2 x_2} - \frac{1}{\sin^2 x_1} \right] \left[ \frac{f(x_2)}{\sin^2 x_2} - \frac{f(x_1)}{\sin^2 x_1} \right] - (\cot x_2 + \cot x_1) \times \\ & \times \left[ \frac{f'(x_2) + \frac{\pi}{4}}{\sin^2 x_2} + \frac{f'(x_1) + \frac{\pi}{4}}{\sin^2 x_1} \right] + \frac{1}{\sin^2 x_1 \sin^2 x_2} \left[ f(x_1 + x_2) + \frac{1}{3} \sin^2(x_1 + x_2) \right] + \\ & + \frac{\pi}{8} [g(x_1) + g(x_2)], \end{aligned} \quad (4)$$

where  $f'$  denotes the derivative of  $f$  with respect to its argument. Explicitly, the auxiliary functions  $f$ ,  $f'$ , and  $g$  are given by

$$f(x) = 1 - x \cot x - \frac{\pi}{2} \tan \frac{x}{2}, \quad (5)$$

$$f'(x) + \frac{\pi}{4} = \frac{2x - \sin(2x)}{2 \sin^2 x} - \tan^2 \frac{x}{2}, \quad (6)$$

$$g(x) = \left[ 1.5 + \tan^2 \frac{x}{2} + 0.3 \tan^4 \frac{x}{2} \right] \tan \frac{x}{2} + \frac{2}{\sin^3 x}. \quad (7)$$

We remark that the above expression for Coulomb energy is the exact solution of Poisson's equation for a uniform charge distribution of the system [61].

For the surface potential energy we have introduced an effective surface tension,  $\sigma_{\text{Eff}}$ , to the deformed system, defined through the equation

$$\frac{3}{5}e^2 \left[ \frac{Z_p^2}{R_p} - \frac{Z_1^2}{R_1} - \frac{Z_2^2}{R_2} \right] + 4\pi\sigma_{\text{eff}}(R_p^2 - \bar{R}_1^2 - \bar{R}_2^2) = Q, \quad (8)$$

where  $Z_{ie}$  ( $i = p, 1, 2$ ) are the nuclear charges, respectively, of the parent, emitted, and daughter nuclei. This definition establishes that the difference between the energies of the initial and final configurations of the system reproduces the energy released in the disintegration, the  $Q$ -value, defined as  $Q = M - M_1 - M_2$ . The mass-values in the  $Q$ -value expression have been taken from the atomic mass evaluation by Audi *et al.* [57] when available, otherwise from the tables by Möller *et al.* [58]. Therefore, for the surface potential energy we have

$$V_s = \sigma_{\text{eff}}(S_1 + S_2), \quad (9)$$

where the surface of each spherical segment is given by

$$S_i = \pi R_i(R_i + \delta_i), \quad (10)$$

in which

$$\delta_i = \begin{cases} \zeta - \xi, & i = 1 \\ \xi, & i = 2 \end{cases}. \quad (11)$$

The effect of the centrifugal potential energy after the scission point has been introduced as usually by the expression

$$V_l = \frac{\hbar^2 l(l+1)}{2\bar{\mu} \zeta^2}, \quad (12)$$

where  $\bar{\mu} = M_1 M_2 / (M_1 + M_2)$  is the reduced mass of the system in the final configuration. Therefore, the effective, one-dimensional total potential energy reads

$$V = V_c + V_s + V_l, \quad (13)$$

subject to the constraints given by Eqs. (1) and (2), and the constraint which defines the mass transfer through the contact window.

### GAMOW'S FACTOR AND DECAY HALF-LIFE

The quantum transition rate from the initial to the final state of the system has been determined by reducing the problem to a one-dimensional motion like in Gamow's alpha-decay theory. The penetrability factor is calculated under the assumption that the system tunnels a barrier of height  $V - Q$ . Shell effects, which appear in the  $Q$ -value [already used in Eq. (8)], act directly on the height and width of the effective barrier. The penetrability factor is calculated by

$$\mathcal{P} = \exp \left[ -\frac{2}{\hbar} \int_{\zeta_0}^{\zeta_c} \sqrt{2\mu[V(\zeta) - Q]} d\zeta \right]. \quad (14)$$

The limits of integration are the inner turning point

$$\zeta_0 = R_p - \bar{R}_1, \quad (15)$$

and the outer one, which, for  $l = 0$ , is given by

$$\zeta_c = Z_1 Z_2 e^2 / Q. \quad (16)$$

Finally, the half-life is calculated as

$$\tau = \frac{\ln 2}{\lambda} \quad (17)$$

with

$$\lambda = \lambda_0 \mathcal{P}, \quad (18)$$

where  $\lambda_0$  is a parameter of the model associated with the time scale of cluster preformation (in the case of cluster emission), or the surface oscillation characteristic time for the fission process.

## NUCLEAR RADII AND INERTIA COEFFICIENTS

The final radii of the fragments should be given by

$$\bar{R}_i = \left[ \frac{Z_i}{Z_p} \right]^{1/3} R_p, \quad i = 1, 2, \quad (19)$$

to be consistent with the uniform charge distribution considered in the Coulomb potential. The radius of the parent nucleus is determined by the simple formula

$$R_p = r_0 A_p^{1/3},$$

where  $r_0$  is the most significant parameter used to adjust the model to the set of experimental data. Values of  $r_0$  for different applications of the model together with the values of  $\lambda_0$  are presented in Table A.

An additional constraint relationship will distinguish two different descriptions for the mass transfer through the internal window. To characterize the Varying Mass Asymmetry Shape (VMAS) description we regarded the radius of the lighter fragment as constant, i. e.,

$$R_1 - \bar{R}_1 = 0, \quad (20)$$

where  $\bar{R}_1$  is the final radius of the light fragment.

On the other hand, in the Constant Mass Asymmetry Shape (CMAS) description, the volume of each fragment radius is constant, and in terms of the lighter fragment radius the volume conservation gives

$$2R_1^3 + 3R_1^2(\zeta - \xi) - (\zeta - \xi)^3 - 4\bar{R}_1^3 = 0. \quad (21)$$

To determine Gamow's penetrability factor we need to know the inertia coefficient,  $\mu$  [Eq. (14)]. Werner-Wheeler's approximation [60] for the velocity field of the nuclear flow has been largely used in the literature [13,62] to define the inertia tensor coefficient. In this approach the velocity field has been obtained from the solution of the continuity equation by using the incompressibility and irrotationality of the nuclear flow. After reduction to the one-dimensional relative motion of the separating parts, only one component of the tensor becomes relevant. The expression for Werner-Wheeler's inertia coefficient is given by

$$\frac{1}{2} \int \rho \vec{v}^2 dr = \frac{1}{2} \mu_{\text{WW}} \dot{\zeta}^2, \quad (22)$$

where  $\rho$  is the mass density for the system, and  $\dot{\zeta}$  is the relative velocity of the geometric center of the fragments. We can determine Werner-Wheeler's inertia coefficient for two parametrizations, namely,  $\mu_{\text{WW}}^{\text{VMAS}}$  and  $\mu_{\text{WW}}^{\text{CMAS}}$  [13,62].

An alternative proposal for calculating the inertia coefficient has been recently applied in one-dimensional penetrability calculations [26]. By means of a straightforward calculation regarding the constraints mentioned above [Eqs. (1), (2), (20), and (21)], the expression for the effective inertia coefficient reads

$$\mu_{\text{eff}} = \mu \alpha^2, \quad (23)$$

where  $\mu = m_1 \times m_2 / (m_1 + m_2)$  is the reduced mass of the nascent fragments, and  $\alpha$  is a configuration-dependent variable which characterizes the evolution of the system in the molecular phase. For the VMAS description one has

$$\alpha^{\text{VMAS}} = 1 - \frac{2}{\zeta(R_2 - \xi)} [(\zeta - \xi)(\bar{z}_1 + \bar{z}_2) + \bar{z}_1^2 - \bar{z}_2^2], \quad (24)$$

where the variable  $\bar{z}_i$  is given by

$$\bar{z}_1 = \frac{\pi}{4} [R_1^2 - (\zeta - \xi)^2] / v_1 \quad (25)$$

$$\bar{z}_2 = \frac{\pi}{4} [R_2^2 - \xi^2] / v_2, \quad (26)$$

in which  $v_1 = \frac{\pi}{3} [2R_1^3 + 3R_1^2(\zeta - \xi) - (\zeta - \xi)^3]$  and  $v_2 = \frac{\pi}{3} [2R_2^3 + 3R_2^2\xi - \xi^3]$  are the volumes of each spherical segment.

For the CMAS description, where the mass of the fragments does not vary during the molecular phase, we have

$$\alpha^{\text{CMAS}} = 1 + \frac{1}{v_1} [R_1^2 - (\zeta - \xi)^2] \left[ R_1 \frac{dR_1}{d\zeta} - (\zeta - \xi) \left( 1 - \frac{d\xi}{d\zeta} \right) \right] + \frac{1}{v_2} (R_2^2 - \xi^2) \left( R_2 \frac{dR_2}{d\zeta} - \xi \frac{d\xi}{d\zeta} \right), \quad (27)$$

where

$$\frac{d\xi}{d\zeta} = -\gamma \frac{dR_2}{d\zeta}, \quad (28)$$

$$\frac{dR_1}{d\zeta} = \frac{1}{R_1} \left[ (\zeta - \xi) + (R_2 + \gamma\zeta) \frac{dR_2}{d\zeta} \right], \quad (29)$$

$$\frac{dR_2}{d\zeta} = -\frac{(\zeta - \xi)(6R_1 + 4\zeta - 4\xi) + R_1(5R_1 + 3\zeta - 3\xi)}{(R_2 + \gamma\zeta)(6R_1 + 4\zeta - 4\xi) + \gamma R_1(5R_1 + 3\zeta - 3\xi)}, \quad (30)$$

and

$$\gamma = \left( \frac{6R_2 + 4\xi}{5R_2 + 3\xi} \right). \quad (31)$$

In the next section we present the main results obtained with the current model by using the different inertia coefficients detailed above.

## COMPARISON WITH EXPERIMENT

By using the VMAS and CMAS mass-transfer descriptions, and Werner-Wheeler's and the effective inertia coefficients we were able to calculate the half-life values,  $\tau_c$ , for the different decay cases. All possible cases of spontaneous nuclear break-up such that  $-7.30 \lesssim \log_{10} \tau_c [\text{s}] \lesssim 27.50$  and, at the same time,  $\log_{10} (\tau/\tau_c) > -17.0$  ( $\tau$  is the total half-life of the parent nucleus) have been considered. Calculations have been performed for all parent nuclei of experimental mass values available in the atomic mass table evaluation by Audi *et al.* [57]. Whenever a daughter nucleus does not have its mass value listed in the experimental mass table cited above we have used the most recent mass prediction table by Möller *et al.* [58] as input data. The choice for the well-controlled parameters  $\lambda_0$  and  $r_0$  of the ELDM for each decay mode (proton, alpha, cluster emissions and cold fission) has been done such that the quantity

$$\sigma = \sqrt{\frac{1}{N} \sum_{i=1}^N \left[ \log_{10} \left( \frac{\tau_c^i}{\tau_{\text{exp}}^i} \right) \right]^2} \quad (32)$$

is a minimum. Here,  $\tau_{\text{exp}}$  represents the experimental half-life-value, and  $N$  is the number of experimental data for the decay mode under analysis. Thus, as discussed in [22], the values for both parameters  $\lambda_0$  and  $r_0$  have been determined in order to obtain the best agreement with experimental half-life data (Table A).

Concerning the cases of proton emission from nuclei, Fig. 2 shows the half-life-values for the most recent cases observed in proton-rich emitters. Table B reports such data, as well as the calculated half-lives in the framework of the present ELDM descriptions. In most cases a non-null  $\ell$ -value has been chosen to give the best agreement between calculated and measured half-life-values (see Table B). Results show a strong dependence of the half-life on orbital angular momentum of the emitted proton ( $\ell$ ), and agreement with the existing data become very good if a suitable  $\ell$ -value is employed. In Fig. 3 we show the variation of the half-life of proton emission for  $^{156}\text{Ta}$ ,  $^{161}\text{Re}$  and  $^{171}\text{Au}$  proton emitters as a function of the angular momentum, where it is seen an increase of about ten orders of magnitude in the half-lives when the orbital angular momentum varies from 0 to  $10\hbar$ . By adjusting the model parameters for the proton emission cases it results that the model combination VMAS/WW with  $r_0 = 1.39$  fm and  $\lambda_0 = 1.5 \times 10^{21} \text{ s}^{-1}$  is the best choice in order to reproduce the measured half-life (filled circles in Fig. 2). In this way, the differences between calculated and experimental values are not greater than one order of magnitude.

For the sake of comparison with the most recent experimental half-life-values of alpha decay we have depicted results in Fig. 4. We observe that, in spite of using only two parameters in the model, our theoretical results are comparable to those obtained from other available models [71], in which four adjustable parameters are often used in. Also, both the model parametrizations VMAS/WW and VMAS/EFF are able in reproducing quite well ( $\sigma = 0.38$ ) the measured half-lives for the alpha-decay cases. We remark that the effect of the centrifugal barrier on the half-life of the alpha decay is smaller than that for proton emission cases, and it is still smaller for the cases of heavier cluster emission. In Fig.5 we display the variation of the half-life of alpha decay (part a) and of cluster emission (part b) for some experimentally observed decay cases when  $\ell$  takes the values 0 and  $6\hbar$ .

The present ELDM has been used in cluster radioactive processes for all cases of cluster emission varying from carbon to silicon. The calculated half-lives have been compared with the experimental data (Fig. 6). Equally good agreement with the data is observed in the whole range of emitted cluster mass number for the model combinations VMAS/WW and VMAS/EFF, and better than for the CMAS parametrization. Previous systematic studies on most probable nuclear decays by Poenaru *et al.* [14,15] have considered only

the cases for cluster emission modes. An intercomparison between the present and other [14,15] calculated half-life-values is shown in Table C. The present ELDM predictions are seen comparable (within 1-2 orders of magnitude) to those calculated by using the ASAFM routine.

Although many theoretical and experimental studies on cold fission processes [74–76] have been developed in a recent past, we observe that there is not yet a systematic prediction study of the half-life for the possible cases of these processes for heavy parent nuclei.

In a previous work [23] a quite reasonable performance of the ELDM has been achieved in some cases of cold fission process, even considering the values of model parameters  $\lambda_0$  and  $r_0$  as being the same that were adopted for cluster emission processes. In the present work, the values of model parameters for the cold fission process have been redefined in order to better reproduce the most recent half-life experimental results. The parent nuclei considered for this parameter-values evaluation were  $^{238,240,242}\text{Pu}$ ,  $^{248}\text{Cm}$  and  $^{252}\text{Cf}$ , for which nuclei the fragment total kinetic energy released and the half-life have been simultaneously determined (experimental results are given in Refs. [77,78]). Since a high total kinetic energy of fragments have been observed in these fission processes they should be closely related to the cold nuclear fission process which can be described by the present ELDM.

By defining the mass asymmetry as

$$\eta = \frac{A_2 - A_1}{A_2 + A_1}, \quad (33)$$

a cold fission process is, for the purpose of the present work, the nuclear break-up into two fragments of mass numbers  $A_1$  and  $A_2$  ( $A_2 > A_1$ ) such that  $\eta < 0.25$ . In Fig. 7 we represent the predicted total half-life-values of cold nuclear fission following the model parametrization VMAS/WW for all parent nuclei of available mass-values in the 1997 mass table by Audi *et al.* [57] (as before, for daughter nuclei which do not have the mass-value in the referred mass table we have used the most recent mass predictions by Möller *et al.* [58] as input data).

To have a better feeling on how the ELDM works in the cases of fission processes we focused attention on the mass region near spherical fragments. There exists an experimentally explored fission process of some trans-Bk isotopes, for which cases the mass region of the fission fragments is located nearby the double magic  $^{132}\text{Sn}$  isotope, and presenting a high kinetic energy of fragments compared to the systematic increasing observed in ordinary fission processes [77,79] — the bimodal fission process [77]. In some cases the fragment mass distributions were experimentally determined. In Fig. 8 we compare the

measured mass distributions with the predictions from our ELDM. In spite of the fact that the present model only takes into account gross characteristics of cold fission, the location of the experimental maxima is well reproduced for the nuclei that exhibit the bimodal fission process. Our results are extremely peaked in the product mass region in the vicinity of  $^{132}\text{Sn}$  because we are dealing strictly with cold fission processes, while the experimental distributions are inclusive ones in the fragment kinetic energy. This fact may be the reason for the side spreading of the experimental distribution as compared with our theoretical result. The most appropriate experimental distribution to be compared with our result should be exclusive in kinetic energy of fragments, i. e., distributions of fragments with energies very near the Q-value.

Finally, we present in a Table the calculated half-life-results of the four nuclear decay modes discussed above in the framework of the ELDM for the model combination of inertia coefficient and mass transfer description  $\mu_{\text{WW}}^{\text{VMAS}}$ , and under the assumption of null angular momentum (few exceptions are from some cases of proton emission as explained in table B).

#### ACKNOWLEDGMENTS

The authors wish to express their gratitude to the Brazilian FAPESP, FAPERJ, CNPq, CNEN and CLAF for partial support.

## REFERENCES

- 
- [1] H. G. de Carvalho, J. B. Martins, I. O. de Souza, and O. A. P. Tavares, *Ann. Acad. Bras. Ciênc.* **47**, 567 (1975).
- [2] H. G. de Carvalho, J. B. Martins, I. O. de Souza, and O. A. P. Tavares, *Ann. Acad. Bras. Ciênc.* **48**, 205 (1976).
- [3] H. G. de Carvalho, J. B. Martins, and O. A. P. Tavares, *Phys.Rev. C* **34**, 2261 (1986).
- [4] H. J. Rose and G. A. Jones, *Nature (London)* **307**, 245 (1984).
- [5] D. V. Aleksandrov, A. F. Belyatskii, Yu. A. Glukhov, E. Yu. Nikol'skii, B. G. Novatskii, A. A. Ogloblin, and D. N. Stepanov, *Pis'ma Zh. Eksp. Teor. Fiz.* **40**, 152 (1984) [*JEPT Lett.* **40**, 909 (1984)].
- [6] A. Săndulescu and W. Greiner, *J. Phys. G* **3**, L189 (1977).
- [7] A. Săndulescu, H. J. Lustig, J. Hahn, and W. Greiner, *J. Phys. G* **4**, L279 (1978).
- [8] A. Săndulescu, D. N. Poenaru, and W. Greiner, *Fiz. Elem. Chastits At. Yadra* **11**, 1334 (1980) [*Sov. J. Part. Nucl.* **11**, 528 (1980)].
- [9] H. J. Fink, J. Maruhn, W. Scheid, and W. Greiner, *Z. Phys.* **268**, 321 (1974).
- [10] J. Maruhn and W. Greiner, *Phys. Rev. Lett.* **32**, 548 (1974).
- [11] S. S. Malik, S. Singh, R. K. Puri, S. Kumar, and R. K. Gupta, *Pramāna J. Phys.* **32**, 419 (1989).
- [12] G. A. Pik-Pichak, *Yad. Fiz.* **44**, 1421 (1986) [*Sov. J. Nucl. Phys.* **44**, 923 (1986)].
- [13] M. Gonçalves and S. B. Duarte, *Phys. Rev C* **48**, 2409 (1993).
- [14] D. N. Poenaru, W. Greiner, K. Depta, M. Ivascu, D. Mazilu, and A. Săndulescu, *At. Data Nucl. Data Tables* **34**, 423 (1986).
- [15] D. N. Poenaru, D. Schnabel, W. Greiner, D. Mazilu, and R. Gherghescu, *At. Data Nucl. Data Tables* **48**, 231 (1991).
- [16] W. Mollenkopf, J. Kaufmann, F. Gönnenwein, P. Geltenbort, and A. Oed, *J. Phys. G : Nucl. Part. Phys.* **18**, L203 (1992).

- [17] E. Stefanescu, W. Scheid, A. Săndulescu, and W. Greiner, *Phys. Rev. C* **53**, 3014 (1996).
- [18] A. Florescu, A. Săndulescu, C. Cioaca, and W. Greiner, *J. Phys. G* **19**, 669 (1993).
- [19] S. Singh, R.K. Gupta, W. Scheid, and W. Greiner, *J. Phys. G* **18**, 1243 (1992).
- [20] A. Florescu, A. Săndulescu, and W. Greiner, *J. Phys. G* **19**, 1947 (1993).
- [21] O. Rodríguez, F. Guzmán, S. B. Duarte, O. A. P. Tavares, F. García, and M. Gonçalves, *Phys. Rev. C* **59**, 253 (1999).
- [22] O. A. P. Tavares, S. B. Duarte, O. Rodríguez, F. Guzmán, M. Gonçalves, and F. García, *J. Phys. G : Nucl. Part. Phys.* **24**, 1757 (1998).
- [23] S. B. Duarte, O. Rodríguez, O. A. P. Tavares, M. Gonçalves, F. García, and F. Guzmán, *Phys. Rev. C* **57**, 2516 (1998).
- [24] M. Gonçalves, S. B. Duarte, F. García, and O. Rodríguez, *Comput. Phys. Commun.* **107**, 246 (1997).
- [25] S. B. Duarte, M. G. Gonçalves, and O. A. P. Tavares, *Phys. Rev. C* **56**, 3414 (1997).
- [26] S. B. Duarte and M. G. Gonçalves, *Phys. Rev. C* **53**, 2309 (1996).
- [27] V. Avrigeanu, A. Florescu, A. Săndulescu, and W. Greiner, *Phys. Rev. C* **52**, R1755 (1995).
- [28] A. Benoufella, G. Barreau, M. Asghar, P. Audouard, F. Brisard, T. P. Doan, M. Hussonnois, B. Leroux, J. Trochon, and M. S. Moore, *Nucl. Phys. A* **565**, 563 (1993).
- [29] E. Stefanescu, A. Săndulescu, and W. Greiner, *J. Phys. G* **20**, 811 (1994).
- [30] W. Greiner and A. Săndulescu, *J. Phys. G* **17**, S429 (1991).
- [31] M. Asghar, N. Boucheneb, G. Medkour, P. Geltenbort, and B. Leroux, *Nucl. Phys. A* **560**, 677 (1993).
- [32] Y. X. Dardenne, R. Aryaeinejad, S. J. Azstalos, B. R. S. Babu, K. Butler-Moore, S. Y. Chu, J. D. Cole, M. W. Drigert, K. E. Gregorich, J. H. Hamilton, J. Kormicki, I. Y. Lee, R. W. Loughheed, Q. H. Lu, W. -C. Ma, M. F. Mohar, K. J. Moody, S. G. Prussin, A. V. Ramayya, J. O. Rasmussen, M. A. Stoyer, and J. F. Wild, *Phys. Rev. C* **54**, 206 (1996).
- [33] L. Demattè, C. Wagemans, R. Barthélémy, P. D'hondt, and A. Deruytter, *Nucl. Phys. A* **617**, 331 (1997).
- [34] J. H. Hamilton, A. V. Ramayya, J. Kormicki, W.-C. Ma, Q. Lu, D. Shi, J. K. Deng, S. J. Zhu, A. Săndulescu, W. Greiner, G. M. Ter-Akopian, Yu. Ts. Oganessian, G. S. Popeko, A.

- V. Daniel, J. Kliman, V. Polhorsky, M. Morhac, J. D. Cole, R. Aryaeinejad, I. Y. Lee, N. R. Johnson, and F. K. McGowan, *J. Phys G* **20**, L85 (1994).
- [35] J. H. Hamilton, A. V. Ramayya, S. J. Zhu, G. M. Ter-Akopian, Yu. Ts. Oganessian, J. D. Cole, J. O. Rasmussen, and M. A. Stoyer, *Prog. Part. Nucl. Phys.* **35**, 635 (1995).
- [36] G. M. Ter-Akopian, J. H. Hamilton, Yu. Ts. Oganessian, J. Kormicki, G. S. Popeko, A. V. Daniel, A. V. Ramayya, Q. Lu, K. Butler-Moore, W.-C. Ma, J. K. Deng, D. Shi, J. Kliman, V. Polhorsky, M. Morhac, W. Greiner, A. Săndulescu, J. D. Cole, R. Aryaeinejad, N. R. Johnson, I. Y. Lee, and F. K. McGowan, *Phys. Rev. Lett.* **73**, 1477 (1994).
- [37] W. Schwab, H.-G. Clerc, M. Mutterer, J. P. Theobald, and H. Faust, *Nucl. Phys.* **A577**, 674 (1994).
- [38] R. D. Page, P. J. Woods, R. A. Cunningham, T. Davinson, N. J. Davis, A. N. James, K. Livingston, P. J. Sellin, and A. C. Shotter, *Phys. Rev. C* **53**, 660 (1996).
- [39] C. N. Davids, P. J. Woods, H. T. Penttilä, J. C. Batchelder, , C. R. Bingham, D. J. Blumenthal, L. T. Brown, B. C. Busse, L. F. Conticchio, T. Davinson, D. J. Henderson, R. J. Irvine, D. Seweryniak, K. S. Toth, W. B. Walters, and B. E. Zimmerman, *Phys. Rev. Lett.* **76**, 592 (1996).
- [40] S. Hofmann, *Radiochim. Acta* **70/71**, 93 (1995).
- [41] R. D. Page, P. J. Woods, R. A. Cunningham, T. Davinson, N. J. Davis, A. N. James, K. Livingston, P. J. Sellin, and A. C. Shotter, *Phys. Rev. Lett.* **72**, 1798 (1994).
- [42] R. J. Tighe, D. M. Moltz, J. C. Batchelder, T. J. Ognibene, M. W. Rowe, and J. Cerny, *Phys. Rev. C* **49**, R2871 (1994).
- [43] P. J. Woods, T. Davinson, N. J. Davis, S. Hofmann, A. N. James, K. Livingston, R. D. Page, P. J. Sellin, and A. C. Shotter, *Nucl. Phys.* **A553**, 485c (1993).
- [44] K. Livingston, P. J. Woods, T. Davinson, N. J. Davis, S. Hofmann, A. N. James, R. D. Page, P. J. Sellin, and A. C. Shotter, *Phys. Lett.* **B312**, 46 (1993).
- [45] K. S. Toth, D. C. Sousa, P. A. Wilmarth, J. M. Nitschke, and K. S. Vierinen, *Phys. Rev. C* **47**, 1804 (1993).
- [46] A. Gillitzer, T. Faestermann, K. Hartel, P. Kienle, and E. Nolte, *Z. Phys.* **A326**, 107 (1987).
- [47] T. Faestermann, A. Gillitzer, K. Hartel, P. Kienle, and E. Nolte, *Phys. Lett.* **B137**, 23 (1984)

- [48] S. Hofmann, W. Reisdorf, G. Münzenberg, F. P. Hessberger, J. R. H. Schneider, and P. Armbruster, *Z. Phys. A* **305**, 111 (1982).
- [49] O. Klepper, T. Batsch, S. Hofmann, R. Kirchner, W. Kurcewicz, W. Reisdorf, E. Roeckl, D. Schardt, and G. Nyman, *Z. Phys. A* **305**, 125 (1982).
- [50] K. P. Jackson, C. U. Cardinal, H. C. Evans, N. A. Jelley, and J. Cerny, *Phys. Lett. B* **33**, 281 (1970).
- [51] H. Mahmud, C. N. Davids, P. J. Woods, T. Davinson, A. Heinz, G. L. Poli, J. J. Ressler, K. Schmidt, D. Seweryniak, M. B. Smith, A. A. Sonzogni, J. Uusitalo, and W. B. Walters, *Phys. Rev. C* **64**, 031303(R) (2001).
- [52] S. Ówiock, J. Dobaczewski, P. H. Heenen, P. Magierski, and W. Nazarewicz, *Nucl. Phys.* **A611**, 211 (1996)
- [53] S. Ówiock, W. Nazarewicz, and P. H. Heenen, *Phys. Rev. Lett.* **83**, 1108 (1999).
- [54] F. Guzmán, M. Gonçalves, O. A. P. Tavares, S. B. Duarte, F. García, and O. Rodríguez, *Phys. Rev. C* **59**, R2339 (1999).
- [55] A. Guglielmetti, R. Bonetti, G. Poli, P. B. Price, A. J. Westphal, Z. Janas, H. Keller, R. Kirchner, O. Klepper, A. Piechaczek, E. Roeckl, K. Schmidt, A. Plochocki, J. Szerypo, and B. Blank, *Phys. Rev. C* **52**, 740 (1995).
- [56] A. Florescu and A. Insolia, *Phys. Rev. C* **52**, 726 (1995).
- [57] G. Audi, O. Bersillon, J. Blachot, and A. H. Wapstra, *Nucl. Phys. A* **624**, 1 (1997).
- [58] P. Möller, J. R. Nix, W. D. Myers, and W. J. Swiatecki, *At. Data Nucl. Data Tables* **59**, 185 (1995).
- [59] G. Gamow, *Z. Phys.* **51**, 204 (1928).
- [60] D. N. Poenaru, J. A. Maruhn, W. Greiner, M. Ivascu, D. Mazilu, and I. Ivascu, *Z. Phys. A* **333**, 291 (1989).
- [61] M. Gaudin, *J. Phys. (France)* **35**, 885 (1974).
- [62] D. N. Poenaru, W. Greiner, and E. Hourani, *Phys. Rev. C* **51**, 594 (1995).
- [63] P. J. Sellin, P. J. Woods, T. Davinson, N.J. Davis, K. Livingston, R. D. Page, A. C. Shotter, S. Hofmann, and A. N. James, *Phys. Rev. C* **47**, 1933 (1993).
- [64] C. N. Davids, P. J. Woods, D. Seweryniak, A. A. Sonzogni, J. C. Batchelder, C. R. Bingham,

- T. Davinson, D. J. Henderson, R. J. Irvine, G. L. Poli, J. Uusitalo, and W. B. Walters, *Phys. Rev. Letters* **80**, 1849 (1998).
- [65] K. Rykaczewski, J. C. Batchelder, C. R. Bingham, T. Davinson, T. N. Ginter, C. J. Gross, R. Grzywacz, M. Karny, B. D. MacDonald, J. F. Mas, J. W. McConnell, A. Piechaczek, R. C. Slinger, K. S. Toth, W. B. Walters, P. J. Woods, E. F. Zganjar, B. Barmore, L. Gr. Ixaru, A. T. Kruppa, W. Nazarewicz, M. Rizea, and T. Vertse, *Phys. Rev. C* **60**, 011301 (1999).
- [66] J. C. Batchelder, C. R. Bingham, K. Rykaczewski, K. S. Toth, T. Davinson, J. A. McKenzie, P. J. Woods, T. N. Ginter, C. J. Gross, J. W. McConnell, E. F. Zganjar, J. H. Hamilton, W. B. Walters, C. Baktash, J. Greene, J. F. Mas, W. T. Milner, S. D. Paul, D. Shapira, X. J. Xu, and C. H. Yu, *Phys. Rev. C* **57**, R1042 (1998).
- [67] R. D. Page, P. J. Woods, R. A. Cunningham, T. Davinson, N. J. Davis, S. Hofmann, A. N. James, K. Livingston, P. J. Sellin, and A. C. Shotter, *Phys. Rev. Lett.* **68**, 1287 (1992).
- [68] R. J. Irvine, C. N. Davids, P. J. Woods, D. J. Blumenthal, L. T. Brown, L. F. Conticchio, T. Davinson, D. J. Henderson, J. A. Mackenzie, H. T. Penttilä, D. Seweryniak, and W. B. Walters, *Phys. Rev. C* **55**, R1621 (1997).
- [69] C. N. Davids, P. J. Woods, J. C. Batchelder, C. R. Bingham, D. J. Blumenthal, L. T. Brown, B. C. Busse, L. F. Conticchio, T. Davinson, S. J. Freeman, D. J. Henderson, R. J. Irvine, R. D. Page, H. T. Penttilä, D. Seweryniak, K. S. Toth, W. B. Walters, and B. E. Zimmerman, *Phys. Rev. C* **55**, 2255 (1997).
- [70] G. L. Poli, C. N. Davids, P. J. Woods, D. Seweryniak, M. P. Carpenter, J. A. Cizewski, T. Davinson, A. Heinz, R. V. F. Janssens, C. J. Lister, J. J. Ressler, A. A. Sonzogni, J. Uusitalo, and W. B. Walters, *Phys. Rev. C* **63**, 044304 (2001).
- [71] B. Buck, A. C. Merchant, and S. M. Perez, *At. Data Nucl. Data Tables* **54**, 53 (1993).
- [72] G. Ardisson and M. Hussonnois, *Radiochim. Acta* **70/71**, 123 (1995).
- [73] A. A. Oglobin, R. Bonetti, V. A. Denisov, A. Guglielmetti, M. G. Itkis, C. Mazzocchi, V. L. Mikheev, Yu. Ts. Oganessian, G. A. Pik-Pichak, G. Poli, S. M. Pirozhkov, V. M. Semochkin, V. A. Shigin, I. K. Shvetsov, and S. P. Tretyakova, *Phys. Rev. C* **61**, 034301 (2000).
- [74] H.-H. Knitter, F.-J. Hamsch, and C. Budtz-Jørgensen, *Nucl. Phys. A* **536**, 221 (1992).
- [75] Yu. V. Pyatkov, V. V. Pashkevich, Yu. E. Penionzhkevich, V. G. Tishchenko, A. V. Unzhakova, H.-G. Ortlepp, P. Gippner, C.-M. Herbach and W. Wagner, *Nucl. Phys. A* **624**, 140 (1997).

- [76] P. Armbruster, Rep. Prog. Phys. **62**, 465 (1999).
- [77] D. C. Hoffman and M. R. Lane, Radiochim. Acta **70/71**, 135 (1995).
- [78] A. Sandulescu, S. Misicu, F. Cârstoiu, and W. Greiner, Phys. Part. and Nucl. **30**, 386 (1999).
- [79] O. A. P. Tavares and M. L. Terranova, Nuovo Cimento **105A**, 723 (1992)
- [80] Nuclear data (NuDat) retrieval program, generated at the Nat. Nucl. Data Centre, Brookhaven National Laboratory, Upton NY (USA), March 1998.
- [81] J. K. Tuli (Ed.), Nucl. Data Sheets **56-82** (1989-1997); J. K. Tuli (Ed.), Nuclear Wallet Cards (6<sup>th</sup> Edition, 2000), Nat. Nucl. Data Centre, Brookhaven National Laboratory (Upton, NY).
- [82] S. Hofmann, V. Ninov, F. P. Heßberger, P. Armbruster, H. Folger, G. Münzenberg, H. J. Schött, A. G. Popeko, A. V. Yeremin, A. N. Andreyev, S. Saro, R. Janik, and M. Leino, Z. Phys. A **350**, 277 (1995).
- [83] S. Hofmann, V. Ninov, F. P. Heßberger, P. Armbruster, H. Folger, G. Münzenberg, H. J. Schött, A. G. Popeko, A. V. Yeremin, A. N. Andreyev, S. Saro, R. Janik, and M. Leino, Z. Phys. A **350**, 281 (1995).
- [84] S. Hofmann, V. Ninov, F. P. Heßberger, P. Armbruster, H. Folger, G. Münzenberg, H. J. Schött, A. G. Popeko, A. V. Yeremin, A. N. Andreyev, S. Saro, R. Janik, and M. Leino, Z. Phys. A **354**, 229 (1996).
- [85] O. A. P. Tavares and M. L. Terranova, Radiat. Meas. **27**, 19 (1997).
- [86] H. Kettunen, J. Uusitalo, M. Leino, P. Jones, K. Eskola, P. T. Greenless, K. Helariutta, R. Julin, S. Juutinen, H. Kankaanpää, P. Kuusiniemi, M. Muikku, P. Nieminen, and P. Rahkila, Phys. Rev. C **63** 044315 (2001).

TABLE A: Model parameter-values used in the calculation of the half-lives of the hadronic decay modes for different model combinations of shape parametrization and inertia coefficient ( $r_0$  in fm;  $\lambda_0$  in  $10^{21} \text{ s}^{-1}$ ).

Model combination <sup>a</sup>	Decay mode							
	Proton emission		Alpha decay		Cluster radioactivity		Cold fission	
	$r_0$	$\lambda_0$	$r_0$	$\lambda_0$	$r_0$	$\lambda_0$	$r_0$	$\lambda_0$
V <sub>MAS</sub> , WW	1.39	1.5	1.34	18	1.37	10	1.39	320
V <sub>MAS</sub> , EFF	1.38	0.5	1.13	40	1.20	10	—	—
C <sub>MAS</sub> , WW	1.38	0.5	1.20	44	1.31	10	—	—
C <sub>MAS</sub> , EFF	1.38	0.5	1.13	18	1.17	10	—	—

<sup>a</sup> V<sub>MAS</sub>  $\equiv$  Varying Mass Asymmetry Shape; C<sub>MAS</sub>  $\equiv$  Constant Mass Asymmetry Shape; WW  $\equiv$  Werner-Wheeler's inertia; EFF  $\equiv$  Effective inertia

TABLE B: Intercomparison between experimental and calculated partial half-life-values ( $\tau$  in seconds) for proton emission from nuclei.

Parent nucleus		experimental		calculated				$\ell^a$
$Z$	$A$	$\log_{10} \tau_{\text{exp}}$	Ref.	$\log_{10} \tau_{\text{WW}}^{\text{VMAS}}$	$\log_{10} \tau_{\text{WW}}^{\text{CMAS}}$	$\log_{10} \tau_{\text{eff}}^{\text{VMAS}}$	$\log_{10} \tau_{\text{eff}}^{\text{CMAS}}$	
51	105	1.70	[42]	2.31	2.64	2.06	2.01	2
53	109	-4.00	[46,47,63]	-4.20	-3.88	-4.46	-4.50	2
55	112	-3.30	[41]	-3.31	-3.00	-3.58	-3.62	2
	113	-4.77	[41,46]	-5.64	-5.33	-5.91	-5.95	2
57	117	-1.58	[51]	—	—	—	—	—
63	131	-1.58	[64]	—	—	—	—	—
67	140	-2.22	[65]	—	—	—	—	—
	141	-2.40	[65]	—	—	—	—	—
69	145	-5.45	[66]	—	—	—	—	—
	146	-0.63	[44]	-0.30	-0.06	-0.69	-0.72	5
	147	0.43	[45,49,63]	0.59	0.83	0.19	0.17	5
71	150	-1.40	[43,63]	-1.34	-1.11	-1.74	-1.77	5
	151	0.89	[48,63]	-1.03	-0.80	-1.44	-1.46	5
73	156	-0.84	[38,67]	-0.48	-0.28	-0.93	-0.95	2
	157	-0.52	[68]	-0.77	-0.57	-1.22	-1.24	0

Parent								
nucleus		experimental		calculated				
$Z$	$A$	$\log_{10} \tau_{\text{exp}}$	Ref.	$\log_{10} \tau_{\text{WW}}^{\text{VMAS}}$	$\log_{10} \tau_{\text{WW}}^{\text{CMAS}}$	$\log_{10} \tau_{\text{eff}}^{\text{VMAS}}$	$\log_{10} \tau_{\text{eff}}^{\text{CMAS}}$	$\ell^{\text{a}}$
75	160	-3.06	[67]	-3.03	-2.84	-3.48	-3.50	2
	161	-3.43	[68]	-3.19	-3.00	-3.64	-3.66	3
77	165	-3.46	[69]	-3.73	-3.53	-4.17	-4.19	5
	166	-0.82	[69]	-0.50	-0.32	-0.98	0.99	2
	167	-0.96	[69]	-1.06	0.89	-1.55	-1.56	0
79	171	-2.65	[69]	-2.74	-2.56	-3.21	-3.23	4
83	185	-4.35	[39]	-4.36	-4.22	-4.89	-4.90	0
		-4.23	[70]					

<sup>a</sup> The reported  $\ell$ -values are those to give the best agreement between calculated and measured half-life-values.

TABLE C: Intercomparison between experimental and calculated partial half-life-values for cluster emission modes of trans-lead parent nuclei.

Parent nucleus		Decay mode		experimental <sup>a</sup>	Half-life-values [ $\log_{10} \tau(s)$ ]				Previous systematics	
$Z$	$A$	$Z_1$	$A_1$		Present systematics <sup>d</sup>				ASAFM <sup>e</sup>	ASAFM <sup>f</sup>
					$\mu_{\text{WW}}^{\text{VMAS}}$	$\mu_{\text{WW}}^{\text{CMAS}}$	$\mu_{\text{eff}}^{\text{VMAS}}$	$\mu_{\text{eff}}^{\text{CMAS}}$		
87	221	6	14	14.46	14.42	13.31	14.24	13.43	15.0	14.3
88	221	6	14	13.41	13.26	12.17	13.13	12.32	14.1	14.2
	222	6	14	11.02	12.02	10.93	11.89	11.09	12.1	11.1
	223	6	14	15.5 <sup>b</sup>	14.24	13.12	14.06	13.25	15.0	15.1
	224	6	14	15.9	16.78	15.64	16.56	15.74	16.9	15.9
	226	6	14	21.3	21.84	20.66	21.54	20.70	21.9	20.9
89	225	6	14	17.15	17.86	16.71	17.64	16.82	18.5	17.8
90	228	8	20	20.87	22.03	20.84	22.18	20.82	21.8	21.9
	230	10	24	24.64	24.78	23.45	25.08	23.24	24.1	25.2
91	231	10	24	23.23	22.00	20.69	22.39	20.58	22.0	23.3

Parent nucleus		Decay mode		Half-life-values [ $\log_{10} \tau(s)$ ]						
$Z$	$A$	$Z_1$	$A_1$	experim <sup>a</sup>	Present systematics <sup>d</sup>				Previous systematics	
					$\mu_{WW}^{VMAS}$	$\mu_{WW}^{CMAS}$	$\mu_{eff}^{VMAS}$	$\mu_{eff}^{CMAS}$	ASAFM <sup>e</sup>	ASAFM <sup>f</sup>
92	232	10	24	21.06	20.48	19.19	20.94	19.14	19.6	20.8
	233	10	24	24.84	23.13	21.81	23.51	21.69	23.5	25.2
	234	10	24,26	25.07	25.51	24.20	25.88	24.03	24.7	26.0
		12	28	25.55	24.86	23.49	25.54	23.27	23.7	25.9
94	236	12	28	21.67	20.33	19.00	21.22	19.01	18.9	21.1
	238	12	28,30	25.70	24.83	23.78	25.87	23.60	23.3	25.9
		14	32	25.28	24.43	23.09	25.65	22.97	22.7	26.1
96	242	14	34	23.15 <sup>c</sup>	21.81	20.61	—	20.79	19.8	23.5

<sup>a</sup> Values taken from Ref. [72].

<sup>b</sup> Mean value from six measurements.

<sup>c</sup> Ref. [73].

<sup>d</sup>  $\mu$  is the inertia coefficient, where VMAS  $\equiv$  Varying Mass Asymmetry Shape; CMAS  $\equiv$  Constant Mass Asymmetry Shape; WW  $\equiv$  Werner-Wheeler's inertia; EFF  $\equiv$  Effective inertia.

<sup>e</sup> Analytical Supersymmetric Fission Model by Poenaru *et al.* [14] with the even-odd effect included.

<sup>f</sup> Analytical Supersymmetric Fission Model by Poenaru *et al.* [15].

**FIGURE CAPTIONS:**

**Fig. 1:** Schematic representation of the dinuclear decaying system. The daughter nucleus and the emitted (smaller) fragment have radius  $R_2$  and  $R_1$ , respectively, and the distance between the geometrical centers of the fragments is denoted by  $\zeta$ . The variable  $\xi$  represents the distance between the center of the heavier fragment and the circular sharp neck of radius  $a$ .

Fig. 2: Half-life of proton radioactivity for proton-rich parent nuclei. Our results (open square,  $\mu_{\text{WW}}^{\text{VMAS}}$ ) agree quite well with the experimental data (filled circle). Significant deviations are seen only in two cases, viz.,  $^{113}\text{Cs}$  and  $^{151}\text{Lu}$  proton emitters. Experimental data are those listed in Table B. The dotted lines are to guide the eyes.

Fig. 3: Angular momentum dependence of the half-life for proton radioactivity. Half-life calculations for  $^{156}\text{Ta}$  (solid line),  $^{161}\text{Re}$  (dashed line) and  $^{171}\text{Au}$  (dotted line) change up to about ten orders of magnitude when orbital angular momentum varies from 0 to  $10\hbar$ . The experimental data are those from Table B.

Fig. 4: The ratio  $\tau_c/\tau_{\text{exp}}$  (in  $\log_{10}$ -scale) of calculated to experimental alpha-decay half-life (points) is plotted versus neutron number of the parent nucleus. Deviation by a factor of 3 between theory and experiment is represented by broken lines. The figure shows the results for the model combination  $\mu_{\text{WW}}^{\text{VMAS}}$ , and  $N = 302$  alpha emitters.

Fig. 5: Effect of the centrifugal barrier on the calculated half-life for alpha decay (a) and cluster emission (b). The solid line represents the half-life for  $\ell = 0$ , and the dashed line for  $\ell = 6\hbar$ . Experimental data are those quoted in Ref. [22] for alpha decay, and from Table C for cluster emission.

Fig. 6: Calculated half-life-values for cluster radioactivity as obtained from the present ELDM with different descriptions for the shape parametrization and inertia coefficients as indicated. Experimental data are those listed in Table C (filled circles).

Fig. 7: Half-lives of cold fission cases as predicted by the VMAS mass transfer description and Werner-Wheeler's inertia coefficient of the present ELDM. Half-life-ranges for cold fission process are indicated by the gray  $\log_{10}$ -scale.

Fig. 8: Calculated fragment-mass distribution in cold fission (histograms) compared to experimental data (full lines) for  $^{258}\text{Fm}$ ,  $^{259}\text{Fm}$ ,  $^{259}\text{Md}$ ,  $^{260}\text{Md}$ ,  $^{258}\text{No}$  and  $^{262}\text{No}$  parent nuclei. The calculated yields (normalized to 1) have been obtained following the VMAS/WW model combination. The experimental yields (also normalized to 1) are obtained from data reported in Ref. [77].

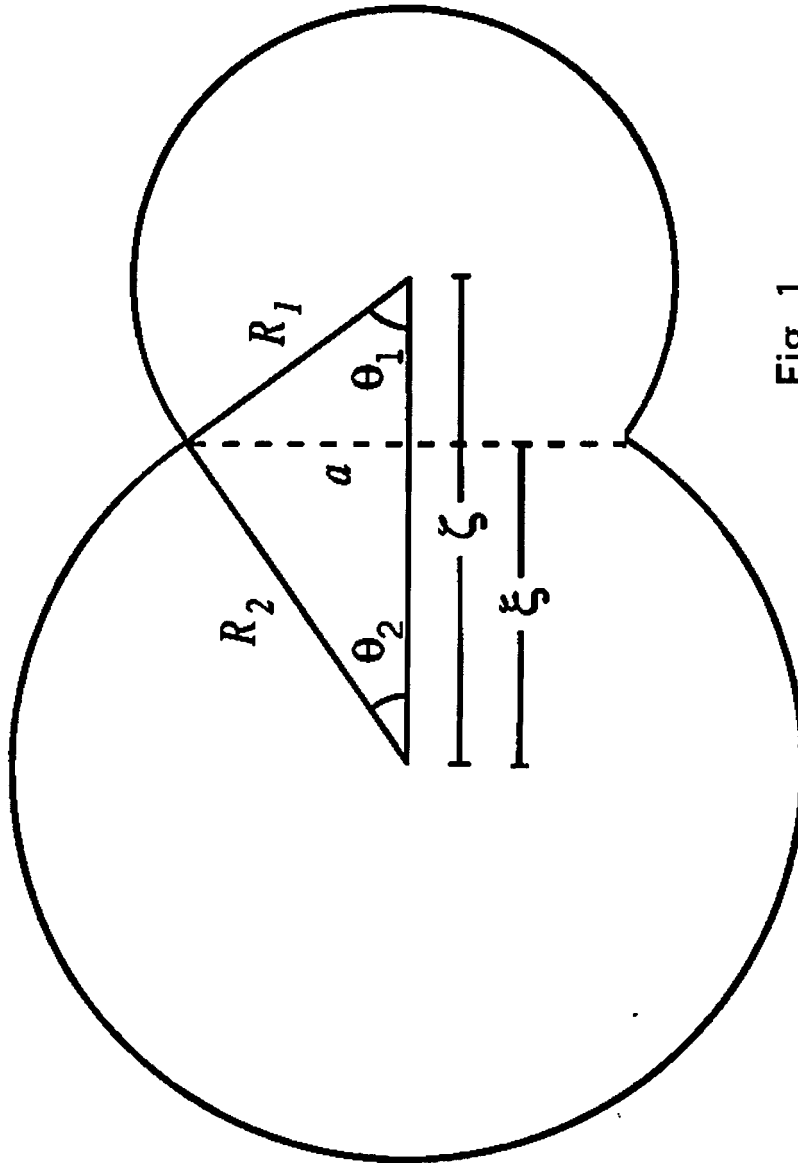


Fig. 1  
Duarte et al.

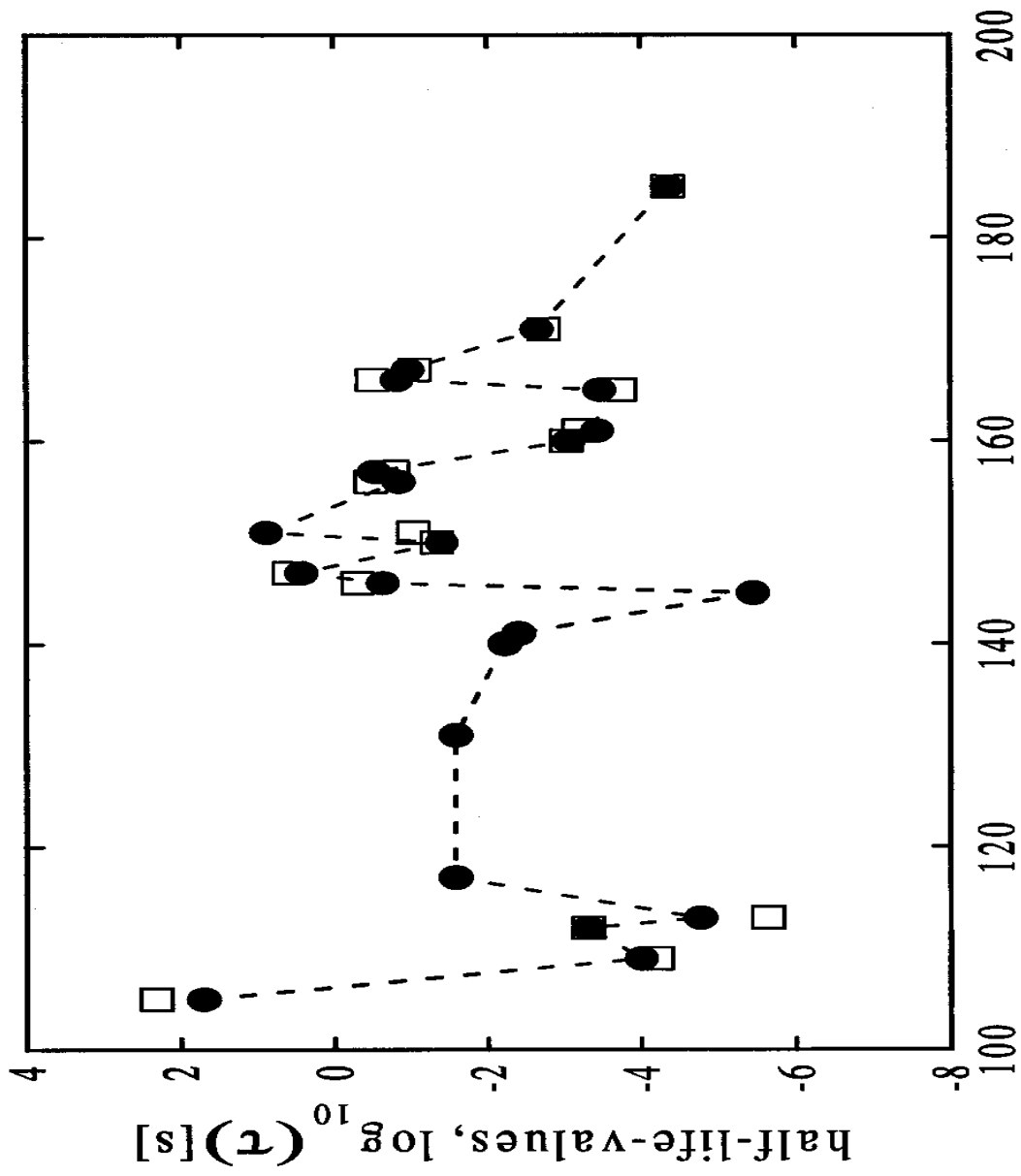


Fig. 2 parent nucleus mass number

Duarte et al.

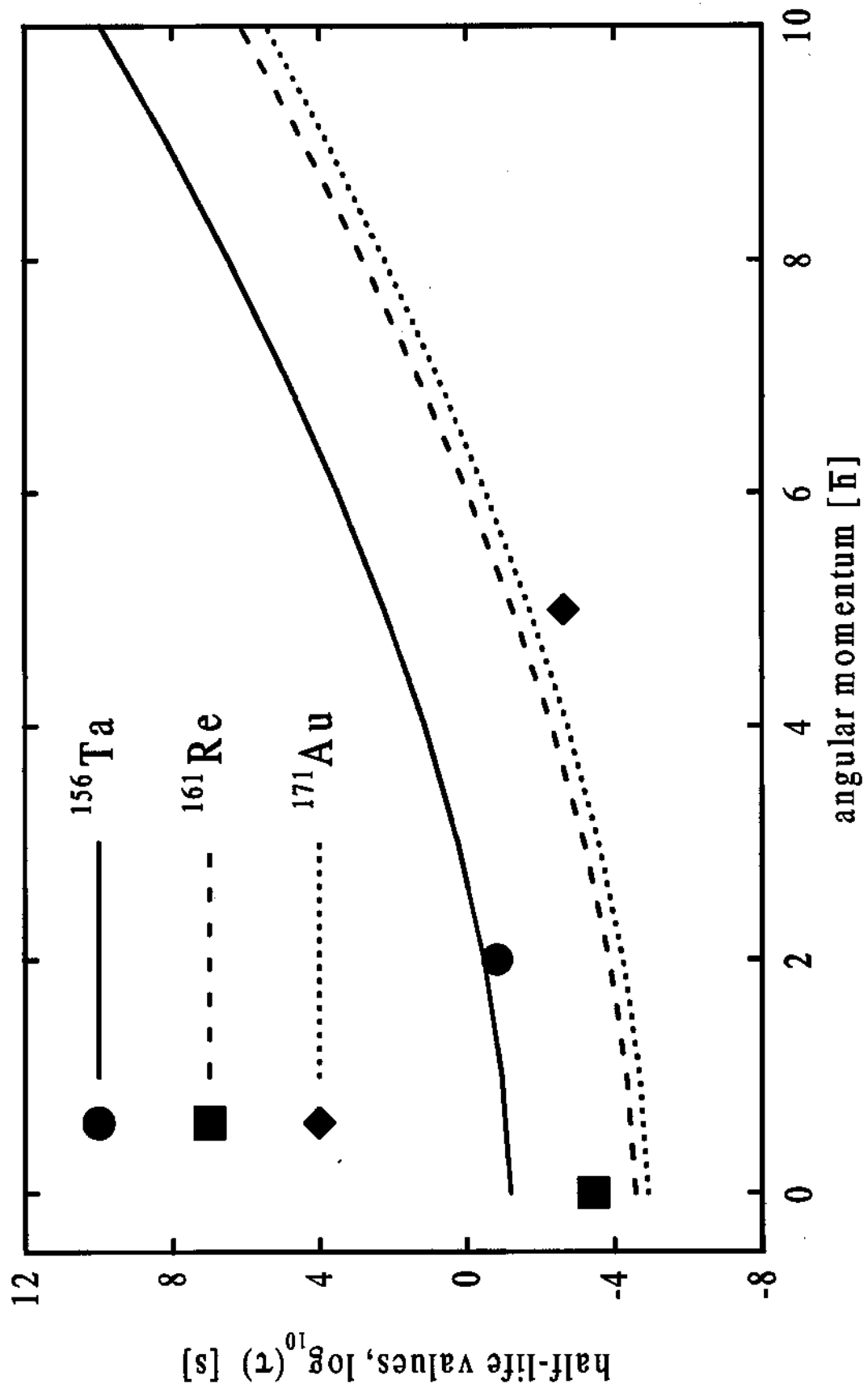
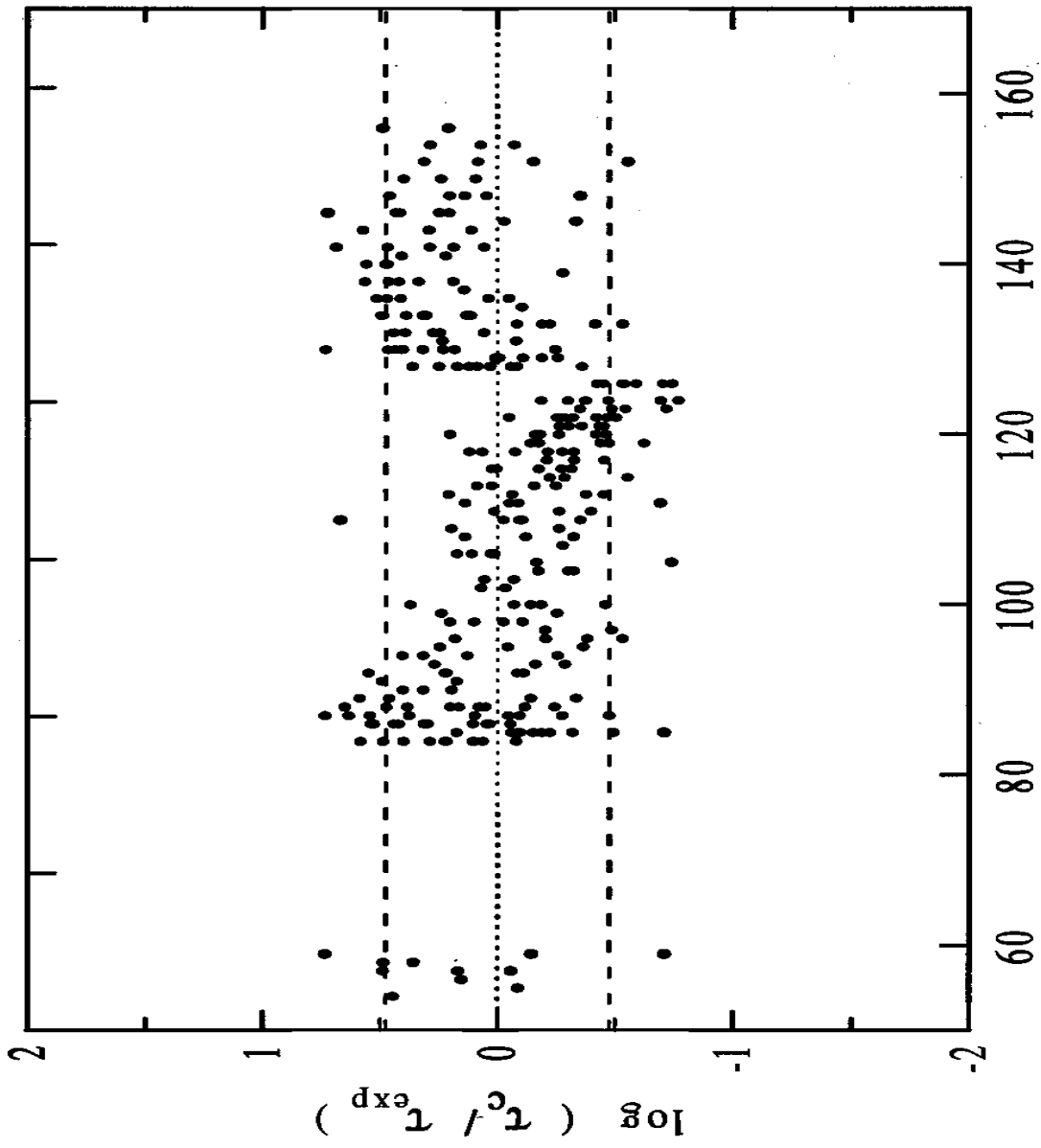


Fig. 3  
Duarte et al.



Parent nucleus neutron number

Fig. 4  
Duarte et al.

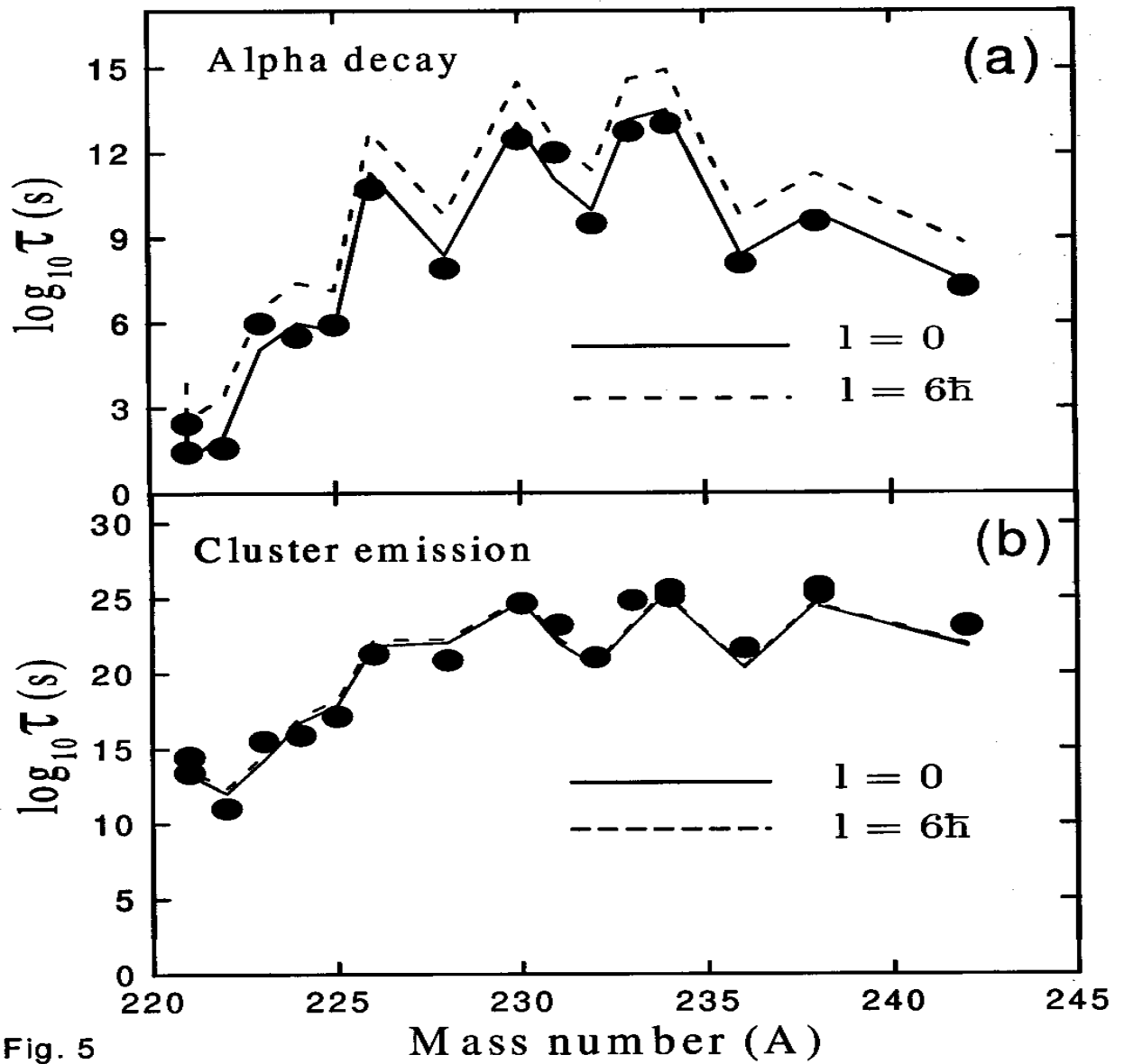


Fig. 5  
Duarte et al.

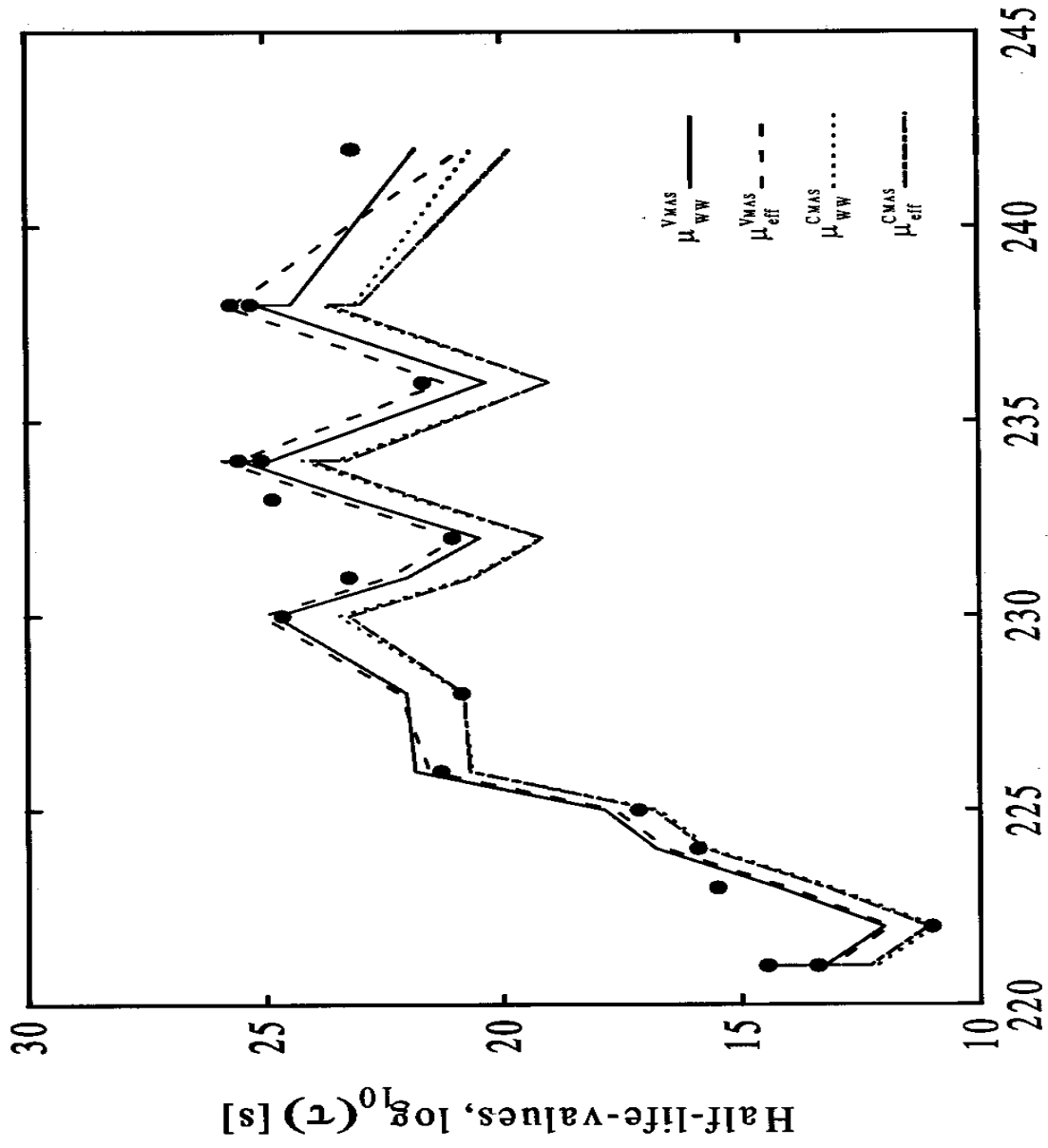
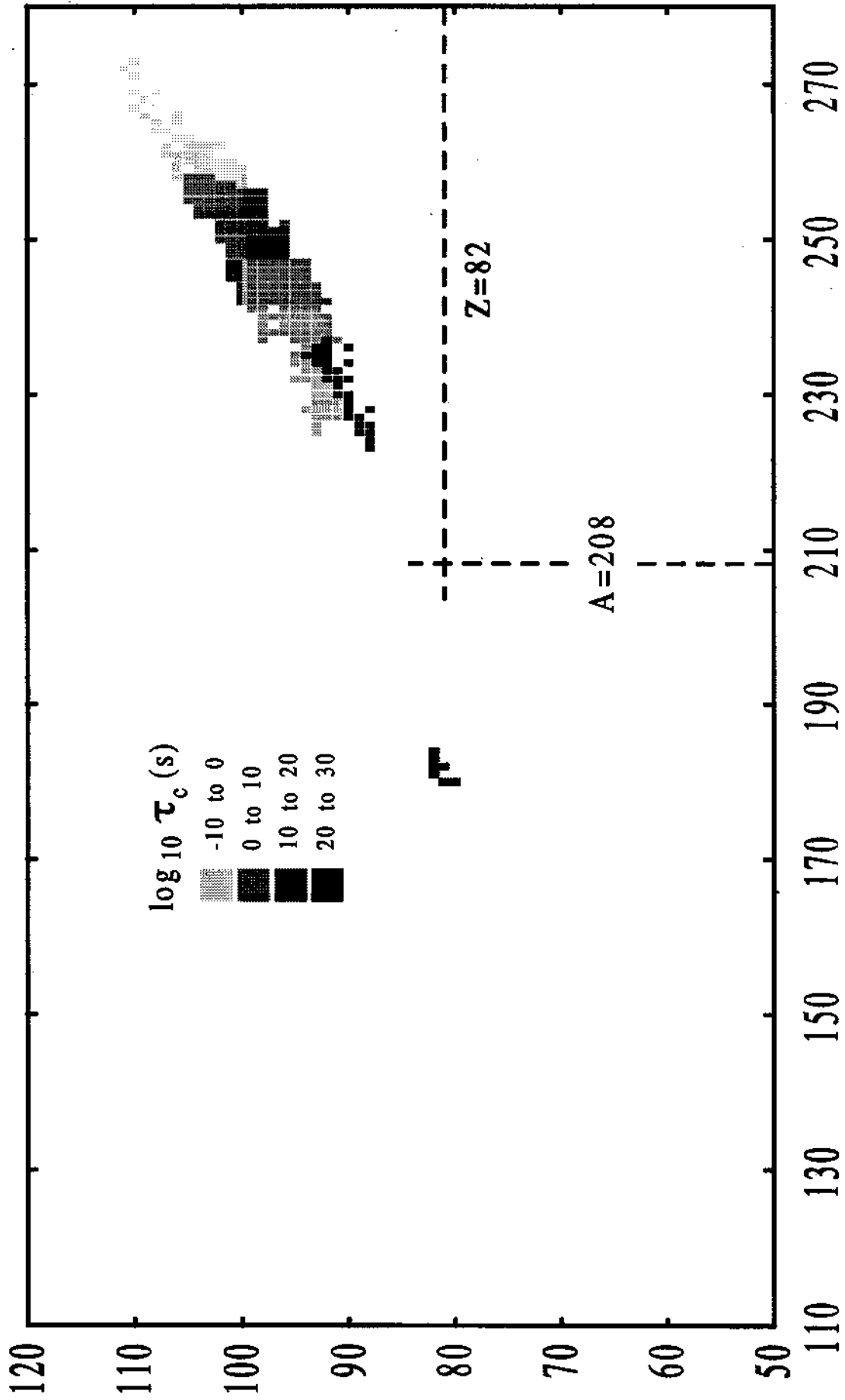
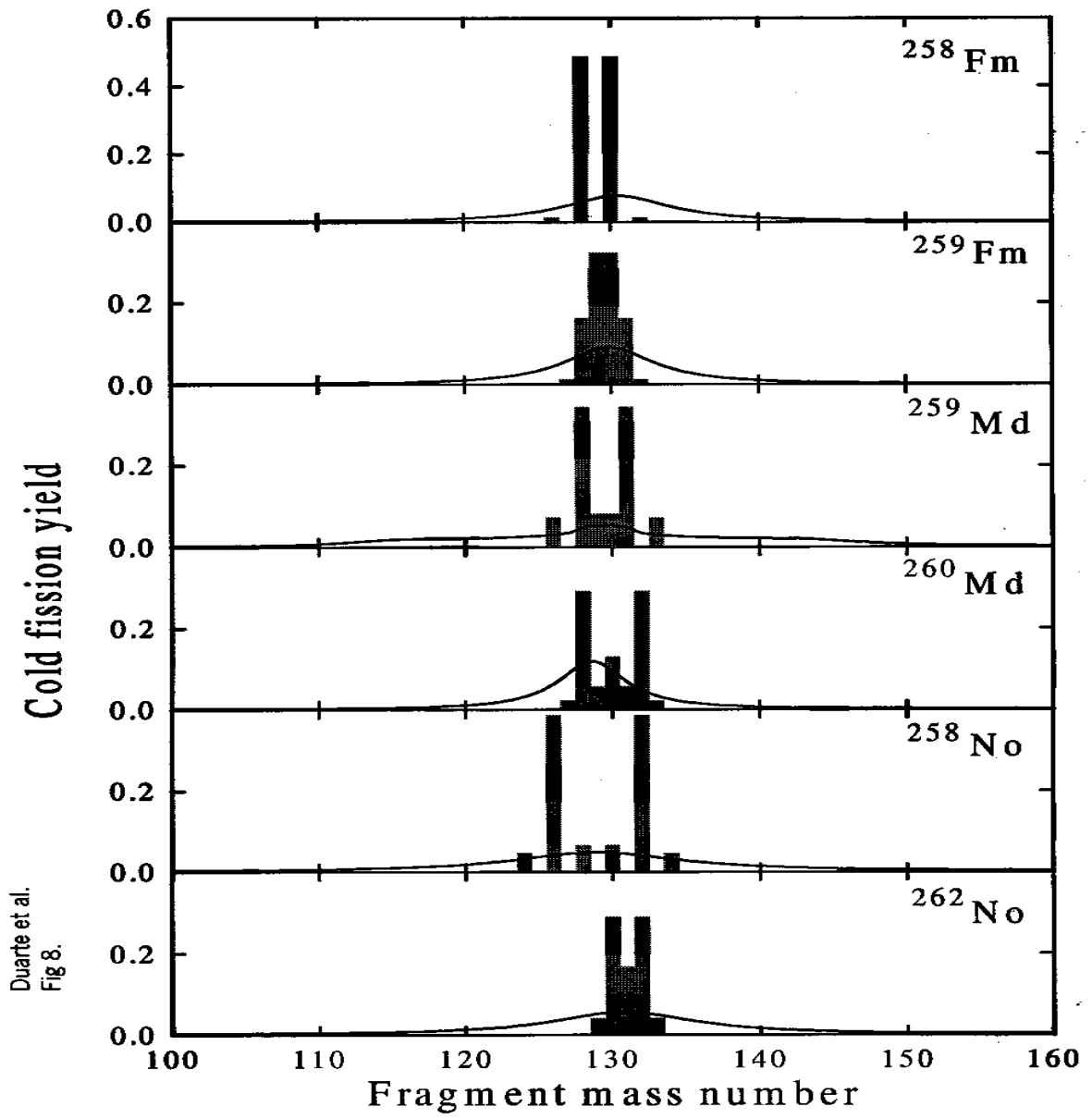


Fig. 6 Parent nucleus mass number

Duarte et al.

Mass number,  $A$ Fig. 7  
Duarte et al.



Duarte et al.  
Fig 8.

## EXPLANATION OF TABLE

**TABLE.** Calculated  $Q$ -values and half-lives for the most probable ground-state to ground-state hadronic decays of nuclei throughout the Periodic Table.

The table lists the calculated  $Q$ -values and half-lives for the most probable hadronic decays (ground-state to ground-state transitions) of nuclei throughout the Periodic Table. The parent nuclei included in this table are those of mass-values available in the Atomic Mass Evaluations by Audi *et al.* [57]. Calculations have been performed according to the shape parametrization VMAS and Werner-Wheeler's inertia coefficient, and under the assumption of null angular momentum ( $\ell = 0$ ). In some cases of proton decay, however, a non-null  $\ell$ -value has been chosen to give best agreement between calculated and measured half-life-values. These  $\ell$ -values are indicated near the calculated results by a superscript following the usual spectroscopic notation, *viz.*, p ( $\ell = 1$ ), d ( $\ell = 2$ ), f ( $\ell = 3$ ), g ( $\ell = 4$ ), and h ( $\ell = 5$ ). Otherwise, the value  $\ell = 0$  is implicit. Decay cases have been selected for calculated half-life,  $\tau_c$  (in second), such that  $-7.30 \lesssim \log_{10} \tau_c \lesssim 27.50$  and  $\log_{10} \left( \frac{\tau}{\tau_c} \right) > -17.0$ , where  $\tau$  is the total half-life of the parent nucleus. Finally, for the cold fission cases, printed here are only the fission modes of mass asymmetry  $\eta \leq 0.04$  (see Eq. (33)).

$Z, Z_1$	Atomic numbers of the parent nucleus and emitted fragment (proton, alpha particle, heavy cluster and/or cold fission fragment), respectively;
$A, A_1$	Mass numbers of the parent nucleus and emitted fragment, respectively;
$\log \tau$	Decimal logarithm of the total half-life (in second). Half-life-values are taken from The [Lund/LBNL] Nuclear Data Search (Version 2.0, Feb. 1999), Depart. of Physics of the Lund University, and LBNL (Berkeley).
$Q$ -value	Total energy available (in MeV) for the decay mode, as calculated from the Atomic Mass Evaluation by Audi <i>et al.</i> [57]. When the mass-value of a daughter nucleus is not listed in [57] it has been taken from the mass table by Möller <i>et al.</i> [58]
$\log \tau_{\text{exp}}$	Decimal logarithm of the experimental half-life (in second) of the indicated decay mode. The partial, experimental half-life data are those quoted in Table B (proton emission), in Refs. [80–86] (alpha decay), and in Table C (cluster radioactivity).
$\log \tau_c$	Decimal logarithm of the calculated half-life (in second) for the decay mode according to the VMAS parametrization and Werner-Wheeler's inertia coefficient of the present ELDM